Article

Oil Shale In Situ Production Using a Novel Flow-Heat Coupling Approach

Bao Jia* and Zhongwei Huang

Read Online

ACCESS | Metrics & More | Article Recommendations

ABSTRACT: Oil shale development, a significant global energy concern, involves the pyrolysis of kerogen, a process that can heat and contaminate groundwater with pyrolysis products. To address these challenges, this study introduces the ambient-temperature gas in situ heating (ATGIH) method as an alternative to traditional techniques. The ATGIH method establishes a low-temperature gas barrier to prevent water infiltration into the production zone by placing heating holes between the injection and production wells. The effectiveness of the ATGIH method in mitigating groundwater contamination during oil shale development is demonstrated through thermochemically coupled reservoir simulations. The study further discusses how gas injection enhances the flowability of mobile oil and gas phases into production wells and how controlling the Dykstra—Parsons coefficient, a measure of heterogeneity, can mitigate gravity segregation and aggregate viscous fingering issues. Our results show that well spacing is a critical factor in designing oil shale development, with a larger spacing resulting in higher energy efficiency but lower oil recovery rates. Furthermore, the study reveals that porosity decreases while permeability increases during pyrolysis due to thermal cracking and pore structure changes. It also highlights that heterogeneity-induced issues can be alleviated by increasing the correlation length to make the system more homogeneous. Therefore, the ATGIH method represents a key innovation in oil shale development, offering a solution that mitigates groundwater contamination while improving the energy efficiency.
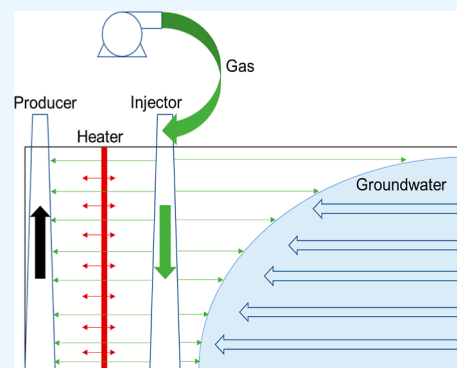
1. INTRODUCTION

Oil shale is a sedimentary rock containing kerogen, a solid organic matter that can be converted to oil and gas through a process called pyrolysis. Large oil shale reserves have been identified worldwide. According to the U. S. Geological Survey estimation, three oil shale deposits, the Piceance Basin, the Greater Green River Basin, and the Uinta Basin in the Green River Formation have oil in place of 1.5, 1.4, and 1.3 trillion, respectively.[1]

Oil shale deposits in China are primarily found in Jilin, Liaoning, and Guangdong provinces, with Jilin being the wealthiest.[2] Oil shale deposits are typically found at shallow depths and have low reservoir temperatures, making them relatively easy to exploit compared to conventional oil and gas reserves. However, the hydrocarbon-bearing porous media in oil shale contain solid, nonflowing kerogen that must be cracked into smaller, flowable hydrocarbon molecules through heating. This process is similar to heavy oil (HO) production in terms of viscosity reduction but requires more energy and higher temperatures due to the nature of oil shale.

Several methods for developing oil shale include traditional surface retorting, which involves mining and crushing the rock and heating it in an internally or externally heated retort oven. While this method is relatively simple to implement, it can produce waste products that are difficult to manage and may contain pollutants such as cyanide and sulfide that can harm the environment. Surface mining for oil shale also requires a large surface area.

Currently, the practical application of oil shale research is focused mainly on in situ conversion methods, where a series of pyrolysis reactions of kerogen occur underground, and the resulting oil and gas products are brought to the surface through wells. This approach requires a smaller surface area compared with traditional surface retorting methods.

One example of an in situ conversion process is Shell's ICP, which uses electric heaters to conduct heat through the oil shale formation and pyrolyze the kerogen into oil and gas.[3] In this technology, well spacing is typically no more than 30 m, and heating holes are distributed in a club-shaped or grid pattern, with the production well located in the center.

Building on in situ methods for oil shale production, various technologies have been proposed and experimented with to

improve efficiency and minimize environmental impact. Notably, ExxonMobil has pioneered a unique technology known as the Electrofrac process.[4] This unconventional in situ conversion method relies on the principle of electrical heating to increase the temperature of oil shale deposits, thus converting kerogen into oil and gas products.

In the Electrofrac process, a conductive heating element is first inserted into a vertical well drilled into the oil shale layer. Electric current is then passed through this heating element, generating heat and raising the temperature of the surrounding rock and kerogen. The generated heat initiates pyrolysis, converting kerogen into hydrocarbon gases and liquids. Unique to this process is the use of an electrical fracture network created by injecting a fracturing fluid into the well, which aids in distributing heat evenly throughout the oil shale formation.

Other organizations are also exploring novel methods for oil shale extraction. For instance, American Shale Oil Corporation has proposed a conduction, convection, and reflux (CCR) technology.[5] Similar to the Electrofrac process, CCR utilizes heating elements inserted into vertical wells to heat oil shale. However, CCR also employs a gravity-driven process, where the resulting hydrocarbon gases rise, condense, and reflux back to heat the untreated oil shale below continually.

Red Leaf Resources, another key player, is advancing a technology called EcoShale In-Capsule Process.[6] This involves mining the oil shale, placing it in a lined surface pit (or "capsule"), and heating the capsule to pyrolyze the shale. While not a strictly in situ process, it offers better environmental control, as the heating and oil recovery are conducted within a sealed capsule, preventing the escape of gases or contaminants into the surrounding environment.

These technologies and Shell's ICP highlight the ongoing efforts to develop efficient, environmentally friendly, and economically viable methods for in situ oil shale production. However, each technology presents its own challenges and trade-offs, indicating a need for further research and innovation in this field.

After heating, traditional oil recovery methods in petroleum engineering can be used to bring crude oil to the surface. In addition to field pilot tests, researchers have also conducted smaller-scale experiments and simulations to explore various techniques for in situ conversion, including the use of high-temperature nitrogen injection and the impact of the heating temperature and wetting properties of porous media on the pyrolysis process. For example, Zhu et al. conducted a study using high-temperature nitrogen injection for oil shale pyrolysis, focusing on the effect of heating temperature and wetting properties of porous media on the process. These simulations were based on a production history matched over a period of 550 days.[7]

Hu et al. conducted experiments to investigate the potential of extracting oil shale using supercritical and subcritical water under isobaric conditions at various temperatures.[8] The researchers compared the solid-to-liquid and solid-to-gas conversion rates and percentages under different conditions. Allawzi et al. studied the effect of mixing hexane and acetone with carbon dioxide on the degree of decomposition of kerogen in Jordanian shale. They found that a higher degree of decomposition was achieved with this method.[9]

Kang et al. investigated the use of $FeCl_3$ and $FeCl_2$ catalysts in subcritical water and found that they were effective at breaking down chemical bonds in heteroatoms, leading to faster decomposition of asphaltene into smaller molecules. The researchers also found that catalysis could enhance the dissolution of carbonates in oil.[7] In addition, Kang et al. tested the use of superheated steam injection in large oil shale samples, with the largest sample measuring 2.2 × 1.7 × 1.1 m and weighing 8.23 tons. The laboratory results showed that this method effectively improved the energy efficiency and oil recovery. Wang et al. from the same institution conducted simulations to study the impact of oil shale anisotropy on the recovery process.[8]

From a modeling perspective, Youtsos developed an in-house code to model the in situ upgrading of oil shale using heated gas injection and conduction heating methods. Their one-dimensional model introduced a series of dimensionless parameters to track the progression of thermal and reaction fronts.[9] Their study found that oil recovery was highly dependent on temperature and gas injection rate but relatively less dependent on operating pressure. Fan et al. used semianalytical and upscaling methods with the Stanford General Purpose Research Simulator.[10] Maes et al. developed an in-house code that mainly examined the interaction between pyrolysis reactions and flow-governing equations.[11] Their results showed that a high Damköhler number, which represents the ratio between the chemical reaction rate and heat diffusion rate, is crucial for efficient pyrolysis.

Several important studies have been conducted to improve the accuracy and efficiency of oil shale pyrolysis simulations. Alpak and Vink, Li et al. from Stanford developed a multiscale approach to enhance the general upscaling scheme, which allows for higher resolution of key in situ heating indicators while maintaining accuracy and reducing computation time by only placing local grid refinement in the vicinity of the wellbore during the in situ heating process.[12,13] Lee et al. used modified TOUGH family simulators and conducted a series of simulations, including a finely gridded system that matched the production data from the Green River oil shale formation.[14] They compared the results of different simulation models using two well-known pyrolysis models. Song et al. used COMSOL finite element modeling to study the in situ pyrolysis of oil shale, using a multilateral well to determine the most efficient well configuration. They found that heat capacity, injection rate, and heating temperature were all critical parameters affecting oil recovery performance.[15]

During in situ cracking, if the shale reservoir is not completely sealed off, the cracked oil and gas can spread outside the production area, leading to resource waste and potential contamination of groundwater resources. Additionally, the energy utilization ratio will decrease if groundwater intrusion occurs due to heat loss. On the other hand, pyrolysis products such as hydrocarbons, cyanides, sulfides, and heavy metal elements can cause irreversible damage to the surrounding environment if they dissolve into groundwater. For example, Hu et al. observed that water soaked in oil shale exhibited strong alkali characteristics and had a peak hydrocarbon concentration after 3 days.

Therefore, to address environmental and economic concerns, it is necessary to isolate the production area during oil shale development. Several methods have been proposed to prevent the loss of oil and gas outside of the production area and prevent groundwater invasion. One such method is Shell's freezing wall technology, which involves drilling around the production area and injecting a refrigerant to create a circular frozen wall, forming an isolation barrier between the production area and the surrounding environment. The frozen wall, liquid refrigerant,

surrounding rock, and connecting pipe network work together to freeze groundwater and prevent the loss of oil and gas beyond the production well. While the freezing wall technology has been successfully applied in the implementation of Shell's ICP technology, it has a long construction period and high operating costs, particularly when the sealing radius is large. Additionally, the freezing wall can cause irreversible damage to the original reservoir structure and alter the pore structure and mechanical properties. Therefore, this method may not be suitable for China's generally low-quality oil shale reserves.

Another method for isolating the production area is the use of a grouting curtain, which involves injecting mud into the surrounding formation through grouped wells in order to seal the reservoir after the mud solidifies. However, similar to the freezing wall technology, the cost of constructing grouting curtains for relatively deeply buried oil shale reserves is high, and the sealing range is limited.

Using gas injection to prevent groundwater invasion is a promising approach for sealing oil shale production areas that does not require high construction costs and utilizes only existing wells. Wells are drilled on either side of the reservoir for gas injection, which acts as a barrier to block groundwater flow toward the production wells. This method has a lower engineering cost and greater flexibility than the traditional freezing wall and grouting curtain techniques, as it does not require the installation of additional underground or surface infrastructure installation.

Sun et al. conducted a simulation using TOUGH2 and the EOS3 model to study the effectiveness of using gas injection to stop water invasion.[16] While this work provides insight into the mechanisms behind this approach, it is necessary to use a more rigorous three-phase model that includes oil, gas, and water to understand the underlying principles fully. Additionally, a significant portion of the energy used during the in situ heating process of oil shale is devoted to heating groundwater, which increases the economic cost. This issue must also be taken into consideration.

Oil shale development involves the pyrolysis of kerogen, a process that can heat groundwater and contaminate it with pyrolysis products.[17−22] Traditional techniques for oil shale development have been associated with significant environmental challenges, including potential groundwater contamination. Current methods for isolating the production area, such as Shell's freezing wall technology or the use of grouting curtains, often require extensive infrastructure, have high operating costs, or can cause irreversible damage to the reservoir structure. These limitations suggest that these methods may not be the most effective or sustainable solutions for preventing groundwater contamination.

In contrast to these traditional techniques, this study introduces a novel approach to oil shale development: the ambient-temperature gas in situ heating (ATGIH) method. The ATGIH method involves placing heating holes between injection and production wells and establishing a low-temperature gas barrier to prevent water infiltration into the production zone. This approach offers several advantages over traditional methods. First, it can be implemented using existing wells, eliminating the need for extensive additional infrastructure. This could substantially reduce the costs associated with the isolation efforts. Second, it has the potential to be a more environmentally friendly solution. By preventing groundwater invasion and minimizing the risk of contamination, this method could reduce the environmental impact of oil shale production.

The structure and research steps of this paper are as follows: First, we establish a three-phase model that couples mass/heat transfer with chemical reactions to simulate the pyrolysis of oil shale. Then, we propose a new method to reduce energy consumption during reservoir heating. Following this, we provide a mechanistic understanding of the integrated approach for producing oil shale formations while simultaneously preventing groundwater intrusion. Finally, we demonstrate the effectiveness of the ATGIH method in mitigating groundwater contamination during oil shale development through thermo-chemical-coupled reservoir simulations.

2. SYSTEM AND MODEL DESCRIPTION

The schematic in Figure 1 illustrates the general sketch for the reservoir and well settings for the ATGIH method in the study.
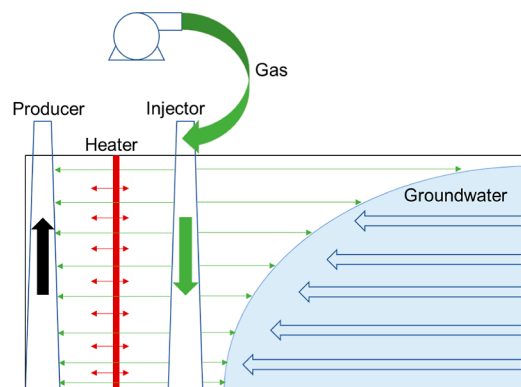

Figure 1. Illustration of the ATGIH method for oil shale in situ pyrolysis. The green and red arrows represent gas and heat flow, respectively.

The figure shows only half of the domain, with the production well on the left and the injector on the right, with heat holes between them. This layout differs from the one used by Sun et al., who did not include heaters or simulate oil production in their model. In the proposed novel approach, low-temperature nitrogen will be directly injected and heated into the production well during convective flow.

The ATGIH method involves the injection of low-temperature nitrogen gas into the production well, which serves as a barrier to prevent groundwater warming on the injector's right side. This approach allows for energy savings and improved economic benefits compared with the injection of high-temperature gas. While nitrogen was used as the primary gas in this study, future research could also consider other types of gas, such as air, CO_2, and steam.

3. SYSTEM SIMULATION

3.1. Oil Shale Pyrolysis Reaction Modeling. Oil shale cracking, or pyrolysis, is a complex process that involves hundreds of chemical reactions. While these reactions can be simplified for the purpose of reservoir simulation, it is important to understand the complexity of the process in order to accurately simulate the gas injection process and understand the mechanisms behind water-stopping. Initially, hydrocarbons exist in the solid form of kerogen in oil shale. To be able to produce oil and gas, kerogen must be cracked into smaller, flowable hydrocarbon molecules through heating. This process, known as pyrolysis, is similar to HO production in that both require the reduction of viscosity through heating (eqs 1 and 2 show the

processes). However, oil shale pyrolysis requires higher temperatures and consumes more energy due to the presence of solid, nonflowing kerogen.

A first-order reaction model is given by

$$v = K \cdot C_i \tag{1}$$

where v is the molar reaction rate (mol/day·m³), K (1/day) is the rate constant dependent on temperature, and C_i is the molar concentration of species i (mol/m³), where K is given by

$$K = K_0 \cdot \exp\left(-\frac{E}{RT}\right) \tag{2}$$

where K_0 (1/day) is frequency factor independent of temperature. E_a is activation energy (J/mol), R is gas constant 8.314 J/(mol·K), and T is temperature (K).

To initiate the calculation of the partial pressure, we first performed phase equilibrium flash calculations. Flash calculations are used to determine the quantity and composition of phases in a system, giving a snapshot of the system's equilibrium state. This step is crucial because it provides the basis for understanding the behavior of the mixture under a specific set of conditions—typically, a predefined pressure and temperature.

The gas/liquid ratio (dimensionless), represented as K_i, gives an indication of the equilibrium between the gaseous and liquid states of the component. This value depends on the nature of the component, the system's temperature, and pressure, and it provides an essential part of the foundation for calculating the partial pressure.

The partial pressure of a specific reactant in the gas phase can be calculated using the gas law, considering the reactant's molar concentrations. The resulting partial pressure is essentially a measure of how much that particular reactant contributes to the total pressure in the system, which provides insights into the reactant's behavior and potential reaction dynamics.

Table 1 shows the four-stage pyrolysis reactions that result in the production of HO, light oil (LO), HCG, prechar, and char, as modified from models of Braun and Burnham (1992).

Table 1. Four-Stage Pyrolysis Reactions That Result in the Production of HO, LO, HCG, Prechar, and Char, Based on the Model of Braun and Burnham (1992)

reaction stage	reaction	reaction frequency factor (1/day)	activation energy (J/mol)
1	kerogen → 0.010699 HO + 0.009722 LO + 0.007131 HCG + 0.640183 prechar	2.59×10^{18}	2.135×10^5
2	HO → 0.661282 LO + 1.503765 HCG + 14.2 prechar	8.64×10^{17}	2.261×10^5
3	LO → 3.237828 HCG + 5.182242 prechar	4.32×10^{16}	2.261×10^5
4	prechar → 0.017177 HCG + 0.99021 char	8.64×10^{17}	2.261×10^5

The core of our ATGIH method is theoretical, which sets the theoretical groundwork for future pilot experiments. To substantiate the feasibility of our new method and authenticate our model, we turn to established models by Braun and Burnham (1992), and an enhanced version of the Wellington model—both widely acknowledged and utilized within the petroleum industry for in situ pyrolysis.

The updated Wellington model that we employed builds upon the original 2005 model (Table 2). This revision

Table 2. Pyrolysis Model of the Modified Wellington Model (Lee et al. 2016)

reaction stage	reaction	reaction frequency factor (1/day)	activation energy (J/mol)
1	kerogen → 0.02691H2O + 0.009815 HO + 0.01755 LO + 0.04002 HCG + 0.01049 H2 + 0.00541 CO2 + 0.5828 prechar	3.74×10^{12}	168105.1854
2	HO(G) → 0.2034 LO + 2.1153 HCG + 16.9188 prechar	7.950×10^{16}	214327.8887
	HO(O) → 1.8269 LO + 0.0402 HCG + 1.8735 prechar	7.950×10^{16}	214327.8887
3	LO(G) → 5.1983 HCG	5.850×10^{16}	228157.0416
	LO(O) → 0.5125 HCG + 11.0771 prechar	5.850×10^{16}	228157.0416
4	HCG → 3.0H2 + 1.8885 char	7.660×10^{20}	323968.6732

recognizes that the kinetics of hydrocarbon generation are a combination of chemical kinetics and mass-transfer resistance, which result in a low apparent activation energy. This comparative analysis serves as an interim validation measure in lieu of direct experimental data.

In the enhanced Wellington model, more specific reactions are observed in the oil or gas phase, and the reaction frequency factors also differ from those in the Braun and Burnham model. We plan to verify the precision of our model by comparing the cumulative oil output and well bottom-hole pressure data predicted by our model to those derived from the Braun, Burnham, and Wellington models. This comparative analysis will strengthen our understanding and confidence in the theoretical underpinnings and the practical applicability of the ATGIH method for oil shale development.

3.2. Formation Model Properties. *3.2.1. Basic Reservoir Parameters.* Given an extensive survey of geological data related to oil shale formations, we have identified the petrophysical properties, of which the initial porosity and permeability are critical. These values cover broad ranges. For instance, a literature survey by Maes et al. (2017),[11] which utilized data from nine research papers, revealed that porosity has a wide range spanning from 0.1 to 0.4, while the initial permeability varies from 10^{-3} mD to 5000 mD.

In our model, we determined the initial porosity and permeability to be 0.3 and 50 mD, respectively. The other parameters listed in Table 3 are also derived from a comprehensive literature survey, with the values largely centering around the median of the data collected from the reviewed literature.

Table 3. Basic Parameters of the Oil Shale Formation

formation thickness, m	32
depth, m	50
original temperature, °C	25
formation compressibility, 1/kPa	7.25×10^{-5}
over/underburden formation volumetric heat capacity, J/(m³·C)	2.35×10^6
over/underburden thermal conductivity, J/(m·day·C)	3.57×10^5
total porosity	0.3
permeability, mD	50

The effective pore space of the oil shale formation is relatively small due to the high concentration of kerogen in the pore space. The effective pore space can be calculated using eq 4

$$V_{\text{eff}} = V_{\text{pore}}(1 - \emptyset_{\text{kerogen}}) \tag{4}$$

where V_{eff} (m^3) is the effective pore space, V_{pore} (m^3) is the total pore space, and Φ_{kerogen} is the volume fraction of kerogen in the pore space.

The oil shale formation is generally buried in relatively shallow depths compared with conventional oil and gas reservoirs; in this study, the average depth is 32 m. Initially, a minimal mobile phase exists in the reservoir, and the solid phase kerogen takes up most of the volume in the pore space; therefore, the effective pore space shrinks, which could be calculated with the formula below (eq 5)

$$\emptyset_{\text{eff}} = \emptyset_{\text{tot}} - \frac{\text{Mass}_{v_{\text{kerogen}}}}{\rho_{\text{kerogen}}} - \frac{\text{Mass}_{v_{\text{prechar}}}}{\rho_{\text{prechar}}} - \frac{\text{Mass}_{v\text{char}}}{\rho_{\text{char}}}$$

$$= \emptyset_{\text{tot}} - \frac{\text{Con}_{\text{kerogen}}\text{M}_{\text{kerogen}}}{\rho_{\text{kerogen}}} - \frac{\text{Con}_{\text{prechar}}\text{M}_{\text{prechar}}}{\rho_{\text{prechar}}}$$

$$\frac{\text{Con}_{\text{char}}\text{M}_{\text{char}}}{\rho_{\text{char}}} \tag{5}$$

where $\text{Mass}_{\text{vkerogen}}$, $\text{Mass}_{\text{vprechar}}$, and $\text{Mass}_{\text{vchar}}$ (kg/m^3) refer to mass per cubic meter for the three components, $\textbf{\textit{Con}}$ (mol/m^3) is the concentration, and $\textbf{\textit{M}}$ (kg/mol) is the molecular weight; ρ_{kerogen}, ρ_{prechar}, and ρ_{char} (kg/m^3) refer to the densities of the three solid phases.

During in situ cracking of oil shale, the effective pore space shrinks as the solid phase kerogen takes up most of the volume in the pores. The amount of shrinkage can be calculated by using this formula.

For oil shale pyrolysis upgrading, due to the multiple-component nature of computation, it is a common practice to use pure components as proxies for the pseudo components. For instance, Maes et al. (2016) applied C_2H_6, $C_{13}H_{28}$, and $C_{37}H_{76}$ for the HCG, low-molecular-weight-oil (LO), and heavy-molecular-weight oil (HO) components,[11] respectively.[23] In our study, we use C_2H_6, $C_{11}H_{24}$, and $C_{22}H_{46}$ as proxies for HCG, LO, and HO, respectively. The properties like critical temperature and pressure are from the National Institute of Standards and Technology (NIST) database. The gas pseudocomponent density is calculated following the method by Maes et al. (2017).[11] For the liquid phase, the density is the reciprocal of the sum of the mass fractions (X_i) of each component divided by their respective densities (eq 6). We determined the densities for each component from their initial densities, taking into account changes in pressure and temperature via their respective compressibility and thermal expansion coefficients (α) (eq 7). As for the solid phase, we neglected both compressibility and thermal expansion; thus, the solid density solely depends on the phase composition (eq 8).

$$\frac{1}{\rho_l} = \sum_i^n \frac{X_i}{\rho_{li}} \tag{6}$$

$$\rho_{li} = f(\rho_{l0i}, p, T, \alpha) \tag{7}$$

$$\rho_s = \rho_{s0} \tag{8}$$

The effective porosity has a linear relationship with the solid concentration according to eq 5. The model is initialized with a

total porosity of 0.3 and a concentration of 1×10^5 mol/m^3. During the in situ heating process, kerogen continues to be consumed, and prechar, char, liquid hydrocarbon, and gas continue to be generated (Figure 2). As a result, the porosity and permeability of the formation evolve dynamically.
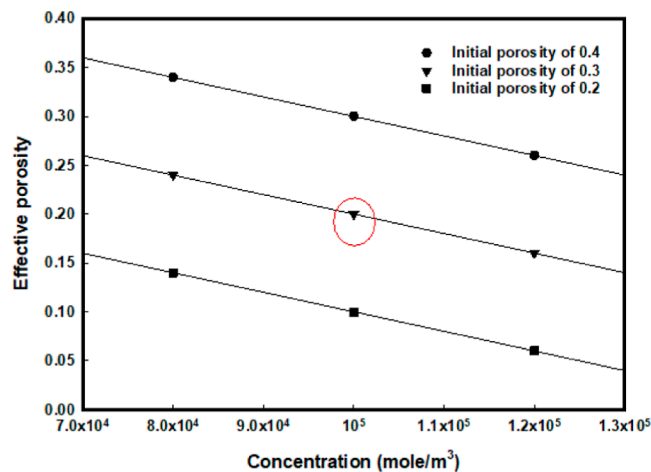

Figure 2. Relationship between effective porosity and kerogen concentration with various initial porosity settings; the red circle indicates the value used in this study.

In order to model the gas/liquid equilibrium in the system, the partitioning coefficient must be calculated. As real lab data are not available for this specific system, empirical values for water, HO, and LO are used. The partitioning coefficient for a given component can be expressed by eq 9

$$K_{\text{pc}} = \left(\frac{kv_1}{p} + kv_2 \times p + kv_3 \right) \times e^{kv_4/T - kv_5} \tag{9}$$

where K_{pc} (dimensionless) is the partitioning coefficient, kv_1 (kPa), kv_4 (°C), and kv_5 (°C) are input for the liquid phases, including the aqueous and oleic phases, using suggested values from Reid et al. to account for the gas–liquid phase equilibrium. kv_2 (1/kPa) and kv_3 (dimensionless) are set to zero while kv_2 and kv_3 are zero (Table 4).[24]

The critical temperature and pressure of H_2O, N_2, and carbon dioxide are derived from the default values in STARS, as these are existing species in the simulator. The properties of HCG, LO, and HO can be determined from the NIST database. It should be noted that the critical properties of the solids are not available and are not required for the simulation.

The thermal conductivity of shale formations can vary widely depending on various factors, with values ranging from 0.4 to 7 W/(m K) for unconsolidated rocks to densely sedimentary rocks. In this study, it is assumed that the thermal conductivity of the shale matrix is constant at 4 W/m/K.

Figure 3 presents the thermal conductivities of the gas, water, and oil phases as obtained from established sources. The overall thermal conductivity is calculated using a linear mixing law of the matrix and three phases, as shown in eq 10

$$\lambda_t = \emptyset[S_w\lambda_w + S_o\lambda_o + S_g\lambda_g] + (1 - \emptyset)\lambda_m \tag{10}$$

where λ_t, λ_o, λ_g, and λ_m are the total, oil, gas, and matrix conductivities, respectively, and S_w, S_o, and S_g are the water, oil, and gas saturations, respectively.

Table 4. Basic Parameters of the Oil Shale Formation

	H2O	HO	LO	HCG	CO₂	N₂	kerogen (solid)	prechar (solid)	char (solid)
molecular weight, g/mol	18.0	310.6	156.3	30.1	44.0	28.0	12.4	11.4	11.0
critical pressure, kPa	22118.4	1248.0	1965.0	4874.6	7377.4	3399.1			
critical temperature, °C	374.2	518.2	365.6	32.3	31.0	−147.0			
KV_1, kPa	1.2×10^7	6.6×10^7	1.4×10^7						
KV_4, °C	−3816.4	−9542.1	−6510.8						
KV_5, °C	−227.0	−273.2	−273.2						
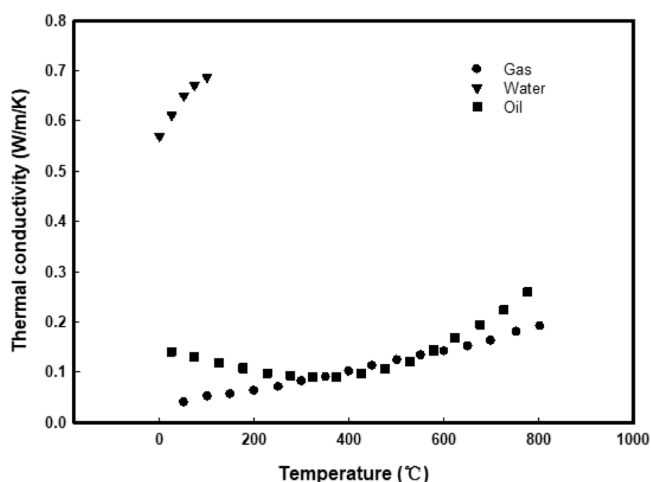
Figure 3. Thermal conductivity of three phases in oil shale formation.

Our study's thermal conductivity of the oil phase of our study was determined using the *n*-Pentadecane (C15H32) alkane as a proxy, as it falls within the range of both LO and HO. This value was calculated using eq 11, with coefficients listed in Table 5.[25]

Table 5. Coefficients in eq 7

a0	168602.599	b1	2119.87
a1	1977.5907	b2	5.3414
a2	−4.371	b3	13901.5
a3	0.0032		
a4	1		
a5	3353.5028		
a6	−2.5282		
a7	0.002		

The overall thermal conductivity of the system was then determined by using a linear combination of the thermal conductivities of the various phases and the rock matrix.

$$\lambda = \frac{a_0 + a_1 T + a_2 T^2 + a_3 T^3 + b_1 p + b_2 p^2}{a_4 + a_5 T + a_6 T^2 + a_7 T^3 + + b_3 p} \tag{11}$$

The liquid viscosity of the three phases (water, HO, and LO) is accounted for using eq 12, where *a* and *b* are in units of cp and °C, respectively. This equation shows that the natural logarithm of the liquid viscosity is proportional to the reciprocal of temperature. The values for the coefficients *a* and *b* for each of the three phases are provided in Table 6.

$$\ln \mu_L = \ln a + b/(T + 273.15)$$

12where μ_L is the liquid viscosity (cp) and T is the temperature (°C).

Table 6. Coefficients a and b in eq 12 for Water, HO, and LO

	water	HO	LO
a, cp	0.0047	0.011	0.011
b, °C	1515.7	3985.4	2201.3

The viscosity of the gas phase is calculated using eq 13, which accounts for the decreasing trend of viscosity as temperature increases. The gas viscosity correlation is given in a generalized form due to a lack of experimental data under the target reservoir conditions.

$$\mu_g = 0.00864 \times (1.574 + 0.0044 \times T) \tag{13}$$

Where μg is the gas viscosity (cp) and T is the temperature (°C).

3.2.2. Relative Permeability and Capillary Pressure. In the simulation of fluid and rock interactions, permeability or, more specifically, relative permeability curves play a vital role. They represent the flow capacity of one fluid phase through a porous medium when other fluid phases are concurrently present.

Typically, relative permeability curves and capillary pressure curves are obtained either through history matching of field data or via experimental methods. However, given the nascent stage of oil shale development, empirical data are significantly scarce. Considering that our main objective is to validate the applicability of our method, we chose to use a standard data set found in the CMG manual for conventional oil reservoirs.

In our model, we require input data for the relative permeability and capillary pressure curves for both the oil/water and liquid−gas systems. The residual and irreducible oil saturations are set to 0.3, indicating that a maximum of 70% oil recovery is achievable in the oil−water phase scenario. In contrast, the residual and irreducible liquid saturations for the liquid−gas system are set to 0, indicating that no liquid will remain during the gas-sweeping process.

In our simulation model, we have designated the system as water-wet and gas-wet, as indicated by the relative permeability curves. When water is the wetting phase, the capillary pressure is calculated as the difference between the oil and water pressures with a positive value reflecting the capillary pressure curves. In the current simulation scenario, water mostly contacts gas, so the gas−liquid relative permeability curve dominates water invasion into the production zone. As the system transitions from gas-wet to liquid-wet, the liquid permeability at a fixed liquid saturation point decreases, leading to a reduction in the water invasion capacity, which could be considered in future studies (Figure 4).

3.2.3. Reservoir Heterogeneity. Reservoir heterogeneity can lead to various fingering phenomena during the two-phase displacement process. To account for this in our model, we generate a range of formation realizations using in-house stochastic synthetic field generators for porosity based on the spectral method with Fourier filtering. The exponential variogram is used, and input parameters for the covariance
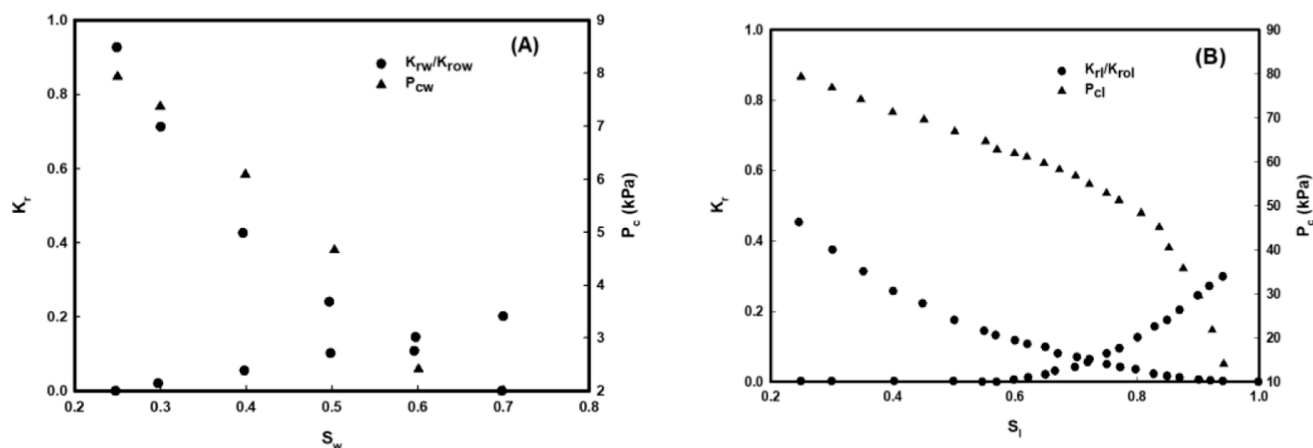
Figure 4. (A) Oil−water and (B) liquid−gas relative permeabilities and corresponding capillary pressure curves.
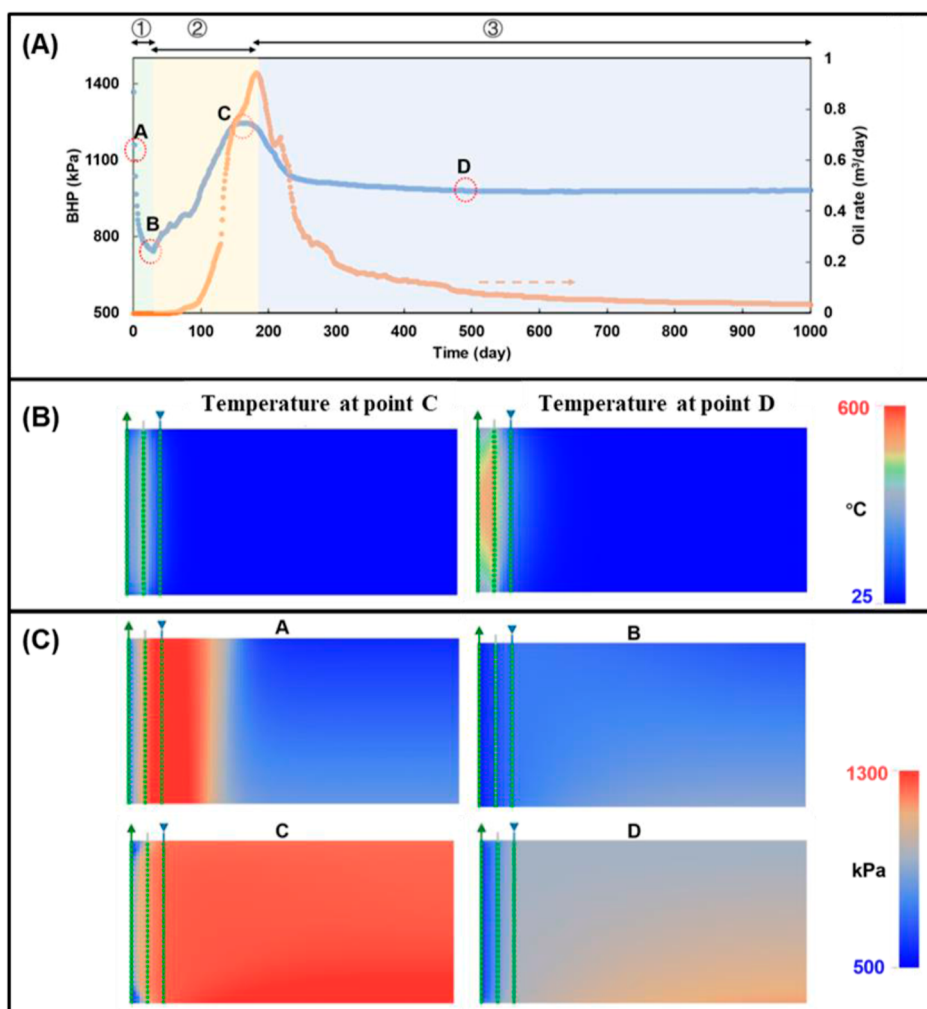

Figure 5. (A) Stages of the proposed ATGIH method: water purging (first stage), compression (second stage), and backflow periods (third stage); (B) temperature distributions at points C and D; and (C) pressure distributions at points A, B, C, and D.

and correlation length in three dimensions are used to generate a series of numbers.

Based on the specified grid dimensions, these numbers are then transformed into a matrix of values by the simulator output, G. Finally, postprocessing is performed to convert the values to lognormally distributed porosity using eq 14, with the specified standard deviation

$$\phi(i, j, k) = \exp \left[\ln \phi_{\text{mean}} + G(i, j, k)\right] \tag{14}$$

A total of nine heterogeneous porosity/permeability scenarios are generated, with varying degrees of heterogeneity and correlation lengths. The degree of heterogeneity is quantified using the Dykstra−Parsons (DP) coefficient, as described in eq 15
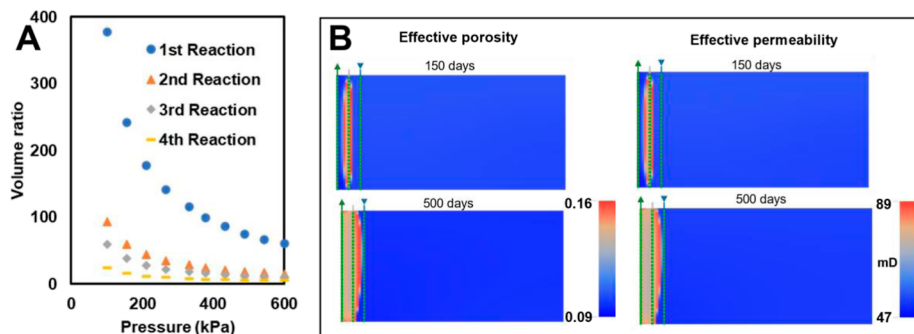
Figure 6. (A) Volume ratio with pressure in different reactions. (B) Evaluation of effective porosity and permeability at 150 and 500 days.

$$\varnothing_{dp} = \frac{\varnothing_{50} - \varnothing_{84.1}}{\varnothing_{50}} \tag{15}$$

where Φ_{50} and $\Phi_{84.1}$ represent the values at the 50 and 84.1% percentiles, respectively.

In the context of a reservoir, correlation length can be used to describe the scale of variability or heterogeneity in a reservoir property, such as porosity, permeability, or saturation. These properties often vary across the reservoir, but they do not do so randomly. Instead, they display spatial correlation: a value at one location is related to the values at nearby locations. The distance over which this relationship holds is defined as the correlation length.

The nine scenarios that we investigate involve DP coefficients of 0.45, 0.65, and 0.85 (considering the range is typically 0.4−0.9) and correlation lengths of 0.5 2.5, and 5 m.

4. RESULTS AND DISCUSSION

4.1. Model Validation. We validated the accuracy of our simulation by comparing the modified Wellington model and the Braun and Burnham (1992) model, employing different reaction models in the pyrolysis of kerogen but maintaining the other parameters of the models constant. By simulating 1000 days of oil and gas production, we found that the discrepancies in oil and gas production and wellbore flowing pressure were within 10%, thus validating our model in this manner.

4.2. Stages of Oil Shale Development. Figure 5 shows the different stages of oil shale development using our innovative approach. In the first stage, nitrogen gas is consistently injected at a fixed rate of 1000 m³/day for an entire month, pushing out groundwater from the reservoir and setting up a state of minimum water saturation within an inert nitrogen environment. As the extraction of groundwater from the formation proceeds, there is a reduction in the average reservoir pressure, implying a decreased bottom hole pressure (BHP) to sustain the same injection rate. At this stage, the pressure propagation displays a piston-like profile because the boundary is still far off, and gravity's effect is negligible.

Owing to gravity segregation, pressure gradually builds up at the bottom right corner, leading to relatively higher-pressure values distanced from the wellbore region. Meanwhile, heat holes start to function at around 600 °C, facilitating kerogen cracking into movable phases, prechar, and char, thus initiating the oil production process.

In the second stage, a combination of porous media variations and an escalating reservoir temperature causes an increase in the average reservoir pressure. Consequently, a higher BHP is required to keep the nitrogen gas flow rate constant. This uptick in BHP aligns with an oil production rate peak at point C. In this

phase, water compression continues, and the pressure propagation pattern remains from the near wellbore region to the bottom right corner. The length of the BHP increase is predicted to depend on the distance between the injection and production wells: a larger distance means more available kerogen for consumption, thereby extending the period of increased BHP.

During the third stage, which is after the oil production peak, the total reservoir pressure begins to decline. The pressure propagation switches from the bottom right to the near wellbore region, paving the way for the potential convective flow of water into the production area, which is shielded by the nitrogen gas barrier.

Examining the temperature distribution profiles at the 1000-day mark, it is clear that heating is confined to the left of the injection well, thereby optimizing energy use by reducing the need to heat surrounding groundwater. Further, the fluid flow pattern from the injection to the production well, driven by the pressure gradient and facilitated by nitrogen as the working fluid, results in an uneven temperature distribution on either side of the heat holes. This uneven distribution is beneficial, as the high-temperature nitrogen near the production well enhances the pyrolysis process, thus contributing to more efficient oil/gas production. Conversely, the low-temperature nitrogen on the injection well side interacts with the water, mitigating heat transfer to the water phase. This kind of placement of the heating holes between the injection and production wells allows the nitrogen to warm during fluid flow, as opposed to the direct injection of high-temperature nitrogen. This method effectively focuses on heating the nitrogen, which directly boosts oil/gas production rather than the surrounding water.

4.3. Porosity and Permeability Evolution. One of the critical factors that determine the efficiency of oil shale pyrolysis is the porosity of the shale, which, in its initial state, has a total porosity of 0.3. This total porosity includes the volume occupied by solids such as kerogen, prechar, char, and other minerals. However, not all of this porosity is available for the flow of oil and gas. The effective porosity, representing the proportion of the total volume available for fluid flow, starts at 0.09.

As the pyrolysis process proceeds, kerogen is gradually consumed, which leads to an increase in the effective porosity. This increase, however, does not reach the level of total porosity (0.3) due to the formation of solid products such as prechar and char, as specified in Table 4.

Figure 6A elucidates the relationship between the reactants and products in terms of their volumes under various pressures. It is notable that under all conditions, the volume ratios are greater than unity. This signifies that the reactions reduce the
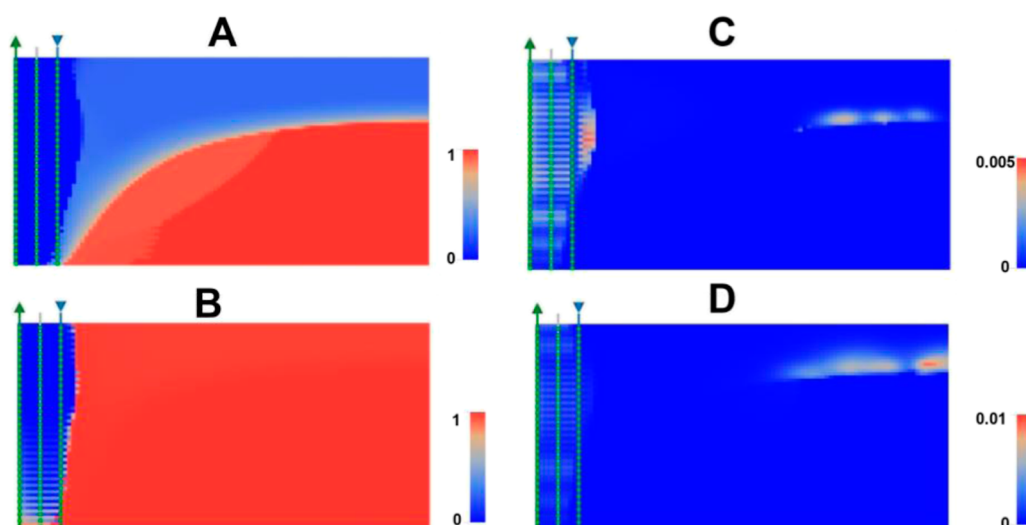
Figure 7. Saturation profiles at the end of 1000 days: (A) water (liquid) saturation, (B) water (global) saturation, and gas hydrocarbon global saturation with gas diffusion coefficients of (C) 5×10^{-4} m²/day and (D) 5×10^{-3} m²/day.

volume of the solid products, thereby leading to an increase in porosity.

The first reaction, in particular, has a profound influence on the porosity and permeability of the shale as its volume ratio is an order of magnitude higher than those of the other reactions.

The permeability of the oil shale changes in correlation with the porosity, as depicted by the Kozeny−Carman equation.[26,27]

Figure 6B shows the evolution of effective porosity and permeability at two distinct time points—150 and 500 days. The changes in porosity and permeability are localized predominantly on the left side of the injection well within the production zones. Similarly, these properties exhibit uneven distributions on either side of the heat holes, mirroring the temperature distributions. It is also observed that the reaction front, indicating the boundary of the heated zone, moves at a faster pace on the production well side.

4.4. Gas as the Water Invasion Barrier. Figure 7A,B depicts the water saturation profile in the liquid and global phases. The global saturation (dimensionless). Global saturation is defined below in eq 12, which considers the gas and liquid phases' saturations.

$$C_i = S_g \times y_i + S_l \times x_i \tag{12}$$

where C_i is the global saturation, S_g and S_l are gas and liquid saturations, respectively; and y_i and x_i are the gas fraction and liquid fraction for species "i", respectively.

Gas-phase water appears at the top of the liquid-phase water due to partitioning effects with a concentration of approximately 25%. The remaining gas component is nitrogen.

Liquid flow is driven by the pressure gradient from the groundwater zone to the production zones; therefore, pyrolysis product hydrocarbons will not be transferred to the aqueous phase through convective mechanisms. However, in addition to partitioning effects, which are accounted for by the gas−liquid partition coefficient, hydrocarbon molecules may also be carried to the aqueous phase through diffusion in the direction of counter-convective flow due to concentration gradients. It should be noted that diffusion occurs in both the gas and liquid phases, but the gas diffusion coefficient is typically several orders of magnitude higher than the liquid diffusion coefficient. Therefore, molecular diffusion should be considered when

evaluating the potential contamination of hydrocarbon groundwater through the gas barrier.

According to previous research by Ghasemi et al., the average diffusivity of ethane and butane in the gas phase of stagnant tank oil and live oil is approximately 6×10^{-5} and 6×10^{-4} m²/day, respectively.[28] Li et al. and Jia et al. reported that the diffusivity of CO_2 in porous media is on the order of 10^{-5} m²/day.[29,30] Using these literature data as a reference, we tested the distance that the most mobile HCG would travel with diffusivity values of 5×10^{-4} and 5×10^{-3} m²/day. The latter value, which is highly unlikely to occur in porous media, was used as a limit to observe the maximum concentration of gas transport into the water zone. Figure 7C,D shows that the HCG transferred through diffusion settles along the gas−liquid interface due to its density, which is higher than that of nitrogen and lower than that of water. The concentration is very low, below 0.5%, and even with the limit value of 5×10^{-3} m²/day, the maximum concentration remains below 1%. Therefore, it can be concluded that the potential for hydrocarbon pollution is sufficiently avoided with the gas-injection-assisted production approach.

4.5. Heterogeneity Impact. Figure 8 illustrates the liquid water saturation profiles in the homogeneous and nine heterogeneous cases over 1000 days. As the correlation length decreases to 0.5 m, which is equal to the vertical grid size and implies that no correlation exists between grids, the number of water fingers increases with the DP coefficient. The fingers become longer and narrower, and more than half of the water zone fingers already reach the production zone, indicating that liquid water has already broken through. The density difference that causes gravity segregation becomes less significant, and the water-swept and nonswept zones are nearly horizontally parallel due to vertical heterogeneity. This means that the water influx into the production zone will not just be from the bottom of the well, as in the homogeneous case. Both the overall cumulative oil and water production decrease, with the water rate being slightly more affected than the oil rate.

As the correlation length increases from 0.5 to 5 m, corresponding to 110 grids, the gas−liquid interface becomes smoother; the hacksaw shape gradually disappears, water fingers become shorter, and water and oil production profiles are closer to the homogeneous case. In summary, the DP-based
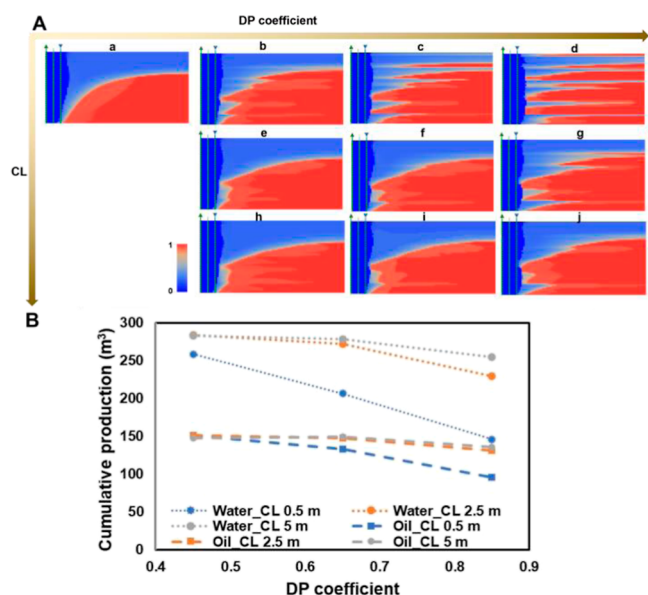
Figure 8. (A) Water (liquid) saturation profiles across different degrees of heterogeneity and correlation lengths, where 'a' represents the homogeneous case, DP coefficient increases horizontally as the arrow indicates (e.g., a → d), and the correlation length increases vertically as the arrow indicates (e.g., a → h). (B) Comparison of cumulative oil and water production across various formation realizations.

heterogeneity impairs both water invasion and oil production, with the former being slightly more sensitive. Under highly heterogeneous conditions, gravity segregation may not be noticeable. A longer correlation length is observed to alleviate the fingering problems caused by heterogeneity.

5. COST ANALYSIS

5.1. Cost Component. Oil shale requires significantly higher energy input compared to other resources due to the need to heat the solid material. In our preliminary economic analysis, we have considered the costs associated with heating and gas compression but have excluded capital costs as we are assuming the utilization of existing wells and surface infrastructure.

The work performed by the gas compressor is modeled as a multistage process, as shown in eq 16

$$w = -\int_1^2 v\,dp = -\int_1^2 \frac{V_1 p_1^{1/n}}{p^{1/n}}\,dp = \frac{n}{n-1}mR(T_1 - T_2)$$

$$= \frac{n}{n-1}mR(T_1 - T_2) = \frac{n}{n-1}mRT_1\left[1 - \left(\frac{p_2}{p_1}\right)^{n-1/n}\right] \tag{16}$$

where n is the polytropic index, T_1 and T_2 are the temperatures before and after compression, and p_1 and p_2 are the pressures before and after compression, respectively. The heat energy, h, is calculated based on the net heat rate provided by the heat holes. The energy source is assumed to be electricity at a cost of 0.08 USD/kWh. The earnings from the oilfield are based on a price of 100 USD per barrel.

Figure 9A illustrates the total cost of oil shale production over 1000 days, consisting of two components: gas compression costs and heating costs. The heating costs, which are the primary constraint on the commercial viability of oil shale production,
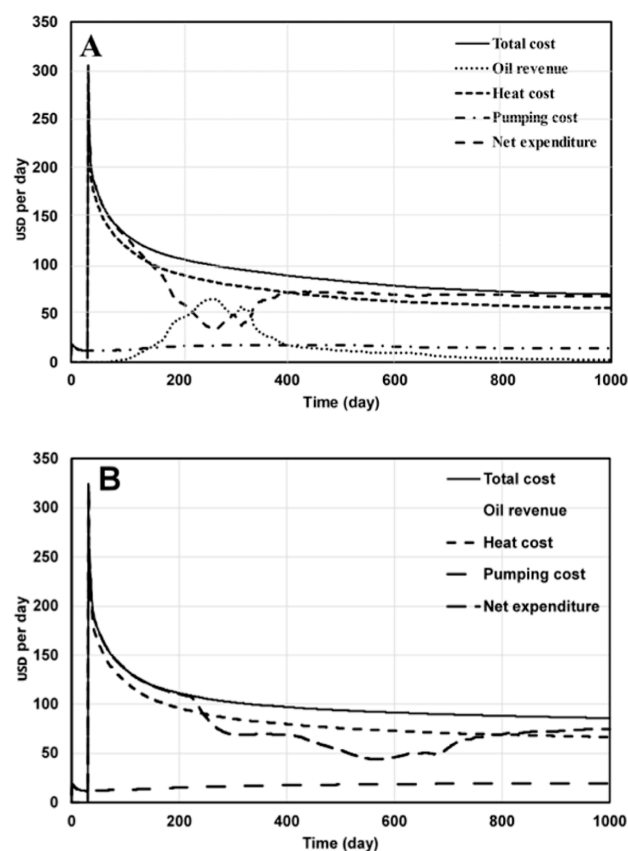

Figure 9. (A) Daily total cost, oil revenue, heat cost, pumping cost, and net expenditure curves and (B) the cost per day by increasing the production zone size by a factor of 2.

are significantly higher at the beginning of production (~300 USD/day) and gradually decrease to ~100 USD/day after about 100 days. In comparison, the gas compression costs are relatively stable and relatively small compared to the heating costs. Oil production begins at around 100 days and reaches its peak at around 270 days, at which point the net expenditure is minimized.

A sensitivity analysis was conducted by increasing the size of the production zone by a factor of 2, resulting in a doubling of the distance between the injection well, heat holes, and production wells. As the production zone is scaled up, oil production begins at around 200 days and reaches its peak at around 500 days due to the longer distance to the production well, which the pyrolyzed oil and gas must travel. The resulting oil production has a longer plateau, in contrast to the original production, which rapidly declines after it reaches its peak. However, the larger production zone also requires higher production inputs, leading to a wider gap between the costs and earnings. This indicates that the spacing of the wells must be carefully considered for an oil shale development project.

5.2. Comparison with the Traditional Method. Figure 10 presents a comparative schematic of the well arrangements using both traditional and novel methods. In the traditional method, two wells are utilized with distances of 20 and 10 m. In the novel method, a heating hole is introduced between the two wells. Both methods exhibit a gas rate of 1000 m³/day. The reservoir properties are consistent between the traditional and the novel methods, as delineated in Table 4.

In the traditional method, gas is directly injected into a hot state, causing the groundwater to be immediately exposed to
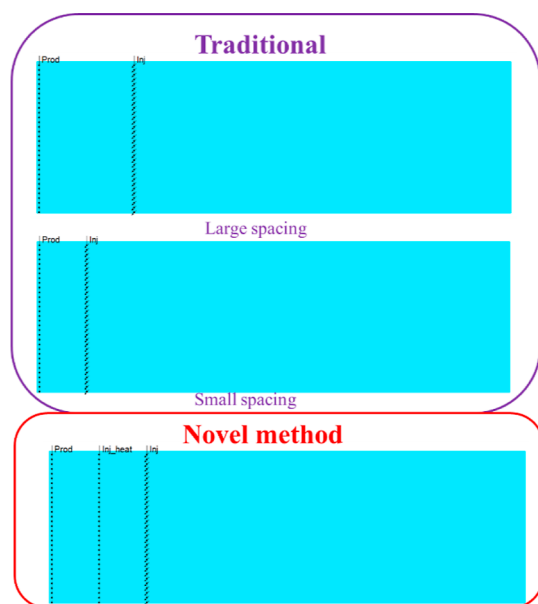
Figure 10. Schematic of the well arrangement in the traditional method, where the injection well directly injects hot temperature gas, versus the novel method, where cold gas is gradually heated using a heater located between the injection well and production well.

high temperatures. In contrast, our novel approach mitigates this direct exposure. Furthermore, to enhance the economic feasibility analysis between the traditional method and our newly proposed strategy, we have set up two different well spacing configurations. This comparison provides meaningful insights into the efficiency and potential advantages of the two approaches, helping to guide the choice of the method for different scenarios. This comparison is also essential for understanding the potential impacts on the surrounding groundwater systems, ultimately contributing to a more sustainable and economically viable approach to well management.

Figure 11 provides a comparative analysis, comprising panels A−D, each displaying different aspects of our simulation results. In panel A, we present the daily and cumulative oil revenue for three different case scenarios. Panel B highlights the daily and total expenses associated with the compressor. Panel C illustrates the overall daily and cumulative costs, while panel D focuses on the daily and total net costs.

Panel A reveals that when the traditional hot gas method and the novel approach we propose are employed with the same spacing, the initiation of oil production in the traditional method experiences a significant delay. Furthermore, the production rate during the same phase is substantially lower, although it continues to grow until day 1000. This phenomenon can be explained by the effective initiation of the pyrolysis process when the heater is placed between the production and injection wells, thus enhancing the permeability of the flowing porous media and simplifying fluid flow.[31]

When the spacing is halved, the fluid travel distance is significantly reduced, resulting in a shorter time to start production. From a cost perspective, as panel B illustrates, smaller spacing leads to lower costs, as it requires maintaining a lower BHP, thus reducing compressor expenses (Figure 12).

The new method avoids heating adjacent groundwater, thereby minimizing heat-related costs. This factor significantly reduces the overall cost, making the new method economically

viable. This is evident in panels C and D of Figure 11, which show that our proposed method incurs the least total and net costs, respectively. Therefore, our proposed method not only accelerates the initiation of oil production and enhances permeability but also achieves considerable cost efficiency, making it a promising approach.

6. SUMMARY AND CONCLUSIONS

In this study, we demonstrated the effectiveness of the ATGIH method for mitigating groundwater contamination during oil shale development through a series of thermochemical-coupled reservoir simulations. The ATGIH method involves the placement of heating holes between the injection and production wells, which is a key innovation compared to previous methods. The method utilizes low-temperature gas as a barrier to prevent water infiltration into the production zone, resulting in improved energy efficiency by avoiding unnecessary heating of groundwater.

This study has several notable advantages. First, the ATGIH method proposed in this study offers a more environmentally friendly solution to oil shale development, as it mitigates groundwater contamination. It also improves the energy efficiency and reduces the costs associated with reservoir heating. Furthermore, the ATGIH method can be implemented using existing wells, eliminating the need for extensive additional infrastructure.

- The ATGIH method consists of three stages: water purging, water compression, and water backflow. Oil production rates increase and decrease in the second and third stages, respectively. The pyrolysis reactions that occur in the production zone lead to a doubling of porosity and permeability, which significantly enhances the flowability of the mobile oil and gas phases into the production well.

- In the presence of layered heterogeneity in the oil shale formation, both oil and water production quantities may decrease, and water infiltration into the production zone may be slightly more affected. However, controlling the DP coefficient can mitigate the impact of gravity segregation and aggregate viscous fingering issues. A longer correlation length also helps to alleviate heterogeneity-induced issues by making the system more homogeneous.

- A cost analysis of the oil shale development project shows that heating the reservoir is the primary expenditure, and it is often difficult to balance the production investment with oil-selling earnings. While expanding the production zone may extend the oil production plateau period, it also delays the onset of oil production and increases both heating and compression costs. Therefore, the scale of the production domain must be carefully evaluated for a pilot or field test of oil shale development.

- Optimizing well spacing for our novel method should balance the immediate benefits of smaller spacing with the long-term production sustainability offered by larger spacing. Factors such as desired return on investment, operational costs, and reservoir characteristics must be considered.

However, there are also disadvantages and limitations of this study. One potential disadvantage is the placement of heating holes between the injection and production wells, which could incur additional costs and, thus, may be seen as a potential
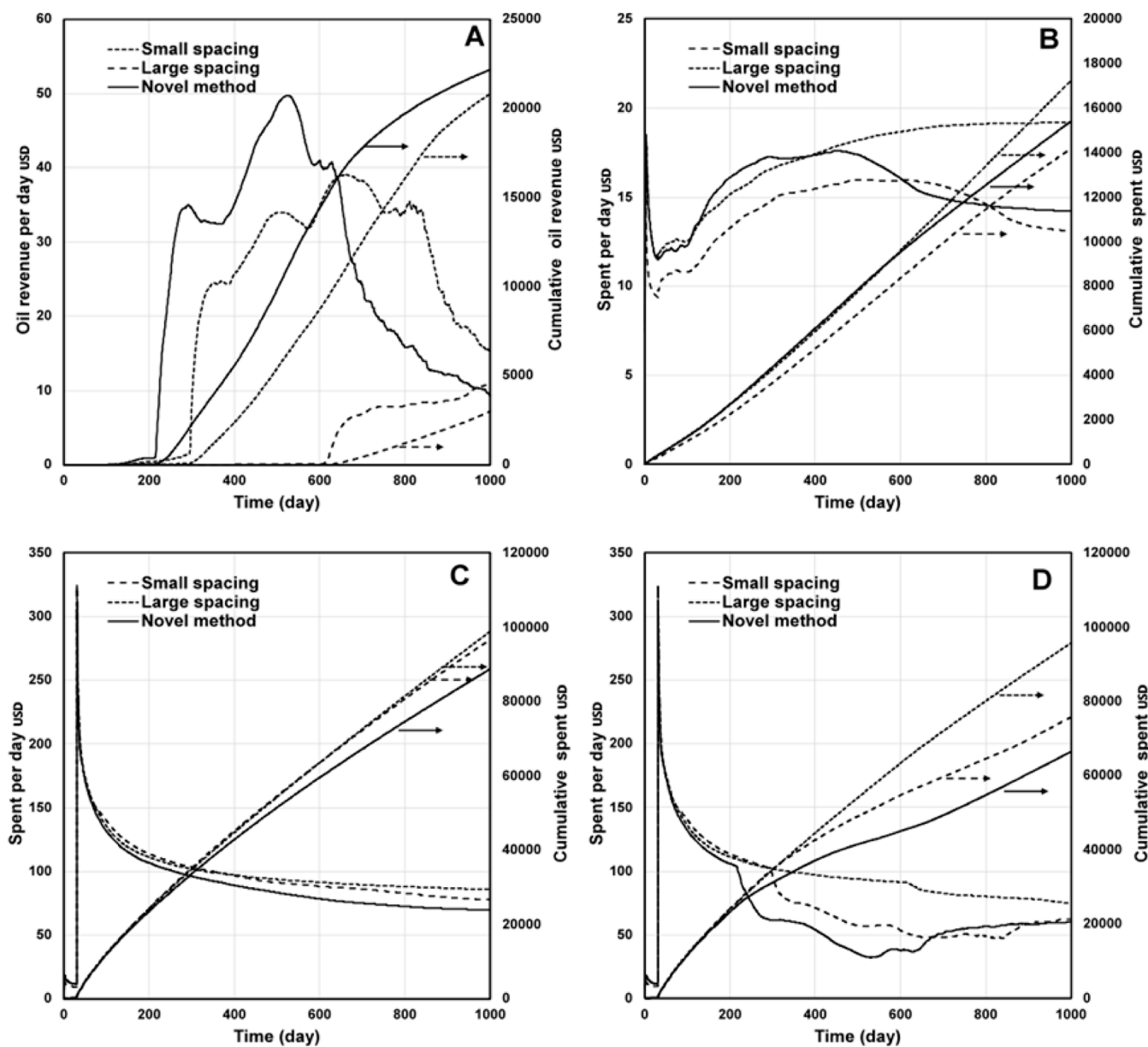
Figure 11. Comparative analysis of daily and cumulative costs and revenues: (A) oil revenue, (B) compressor expenses, (C) total expenditures, and (D) net costs.

drawback. Still, this study provides valuable insights into the potential of the ATGIH method for oil shale development and contributes to ongoing efforts to find more sustainable and economically viable solutions in this field.
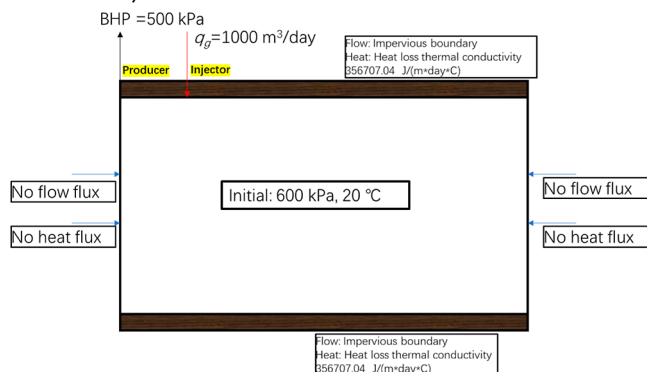
■ APPENDIX

Governing Equation. For a given layer in the model, the governing flow equation for component i in the simulator is given as ref 32

$$\frac{\partial}{\partial t}[V_f(\rho_w S_w w_i + \rho_o S_o x_i + \rho_g S_g y_i) + V_v A d_i]$$

$$= \sum_{k=1}^{n_f} [T_w \rho_w w_i \Delta \Phi_w + T_o \rho_o x_i \Delta \Phi_o + T_g \rho_g y_i \Delta \Phi_g] + V$$

$$\sum_{k=1}^{n_r} (s'_{ki} - s_{ki}) r_k + \sum_{k=i}^{n_f} [\phi D_{wi} \rho_w \Delta w_i + \phi D_{oi} \rho_o \Delta x_i$$

$$+ \phi D_{gi} \rho_g \Delta y_i] + \delta_{iw} \sum_{k=1}^{n_f} \rho_w qaq_{wk} + \rho_w q_{wk} w_i + \rho_o q_{ok} x_i$$
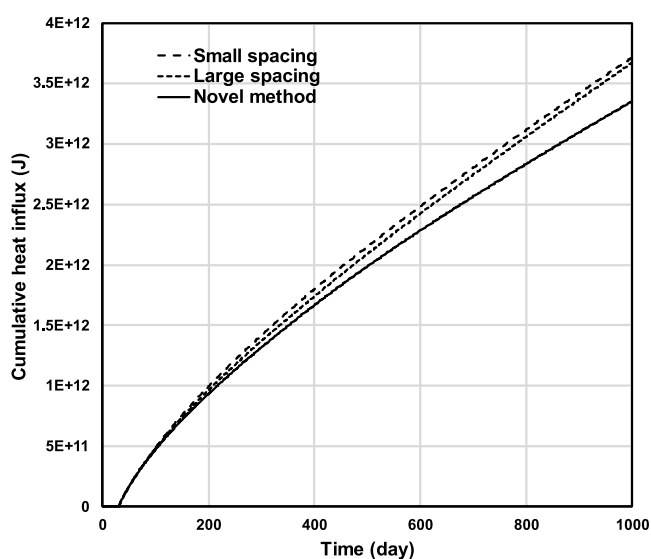
$$+ \rho_g q_{gk} y_i$$

Figure 12. Cumulative heat influx over time under different spacings and using the novel method.

For phase j (w,o,g), the transmissibility is given as

$$T_j = T\left(\frac{k_{rj}}{\mu_j r_j}\right)$$

For layer k, the full energy conversation equation is given as

$$\frac{\partial}{\partial t}[V_f(\rho_w S_w U_w + \rho_o S_o U_o + \rho_g S_g U_g) + v_\nu c_s U_s + V_r U_r]$$

$$= \sum_{k=1}^{n_f} [T_w \rho_w H_w \Delta\Phi_w + T_o \rho_o H_o \Delta\Phi_o + T_g \rho_g H_g \Delta\Phi_g] +$$

$$\sum_{k=1}^{n_f} K\Delta T + \rho_w q_{wk} H_w + \rho_o q_{ok} H_o$$

$$+ \rho_g q_{gk} H_g[\text{well layer } k] + V\sum_{k=1}^{n_r} H_{rk} r_k + HL_o + HL_\nu$$

$$+ HL_c + \sum_{k=1}^{n_f} (HA_{CV} + HA_{CD})_k$$

For the solid component, the governing equation is given as

$$\frac{\partial}{\partial t}[V_v c_i] = V\sum_{k=1}^{n_\tau} (s'_{ki} - s_{ki}) r_k$$

Boundary and Initial Conditions. As shown below, no flow flux is imposed for the overburden and underburden, and the heat loss thermal conductivity is 356707.04 J/(m*day*C). No heat and no heat influx are imposed on the two sides. The injector flow rate is 100 m³/day, and the producer is producing at a constant bottomhole pressure of 500 kPa. Initially, the reservoir is at the same pressure of 600 kPa and temperature of 25 °C.

AUTHOR INFORMATION

Corresponding Author

Bao Jia − *National Key Laboratory of Petroleum Resources and Engineering, China University of Petroleum (Beijing), Beijing 102249, China;* ◉ orcid.org/0000-0003-1953-0696; Email: baojia90@gmail.com

Author

Zhongwei Huang − *National Key Laboratory of Petroleum Resources and Engineering, China University of Petroleum (Beijing), Beijing 102249, China*

Notes

ACKNOWLEDGMENTS

REFERENCES

(1) U.S. Geological Survey Oil Shale Assessment Team. *Oil shale resources of the Eocene Green River Formation, Greater Green River Basin, Wyoming, Colorado, and Utah*; U.S. Geological Survey: Reston, VA, 2011. .

(2) Xu, Y.; Sun, P.; Yao, S.; Liu, Z.; Tian, X.; Li, F.; Zhang, J. Progress in exploration, development and utilization of oil shale in China. *Oil Shale* **2019**, *36* (2), 285.

(3) Meijssen, T.; Emmen, J.; Fowler, T. In-situ oil shale development in Jordan through ICP technology. In *Paper presented at the Abu Dhabi International Petroleum Exhibition and Conference*; SPE, 2014; p D021S023R002. .

(4) Foltin, J. P.; Lisboa, A. C. L.; de Klerk, A. Oil shale pyrolysis: conversion dependence of kinetic parameters. *Energy Fuels* **2017**, *31* (7), 6766−6776.

(5) Mulchandani, H.; Brandt, A. R. Oil shale as an energy resource in a CO2 constrained world: the concept of electricity production with in situ carbon capture. *Energy Fuels* **2011**, *25* (4), 1633−1641.

(6) Bauman, J. H.; Deo, M. Simulation of a conceptualized combined pyrolysis, in situ combustion, and CO2 storage strategy for fuel production from Green River oil shale. *Energy fuels* **2012**, *26* (3), 1731−1739.

(7) Kang, S.; Sun, Y.; Qiao, M.; Li, S.; Deng, S.; Guo, W.; Li, J.; He, W. The enhancement on oil shale extraction of FeCl3 catalyst in subcritical water. *Energy* **2022**, *238*, 121763.

(8) Wang, G.; Yang, D.; Kang, Z.; Zhao, J.; Lv, Y. Numerical investigation of the in situ oil shale pyrolysis process by superheated steam considering the anisotropy of the thermal, hydraulic, and mechanical characteristics of oil shale. *Energy Fuels* **2019**, *33* (12), 12236−12250.

(9) Youtsos, M. S. K.; Mastorakos, E.; Cant, R. S. Numerical simulation of thermal and reaction fronts for oil shale upgrading. *Chem. Eng. Sci.* **2013**, *94*, 200−213.

(10) Fan, Y.; Durlofsky, L. J. J.; Tchelepi, H. A. A. Numerical simulation of the in-situ upgrading of oil shale. *SPE J.* **2010**, *15* (02), 368−381.

(11) Maes, J.; Muggeridge, A. H.; Jackson, M. D.; Quintard, M.; Lapene, A. Scaling analysis of the In-Situ Upgrading of heavy oil and oil shaleding of heavy oil and oil shale. *Fuel* **2017**, *195*, 299−313.

(12) Alpak, F. O.; Vink, J. C. Rapid and accurate simulation of the in-situ conversion process using upscaled dynamic models. *J. Pet. Sci. Eng.* **2018**, *161*, 636−656.

(13) Li, H.; Vink, J. C.; Alpak, F. O. A dual-grid method for the upscaling of solid-based thermal reactive flow, with application to the in-situ conversion process. *SPE J.* **2016**, *21* (06), 2097−2111.

(14) Lee, K. J. Rigorous simulation model of kerogen pyrolysis for the in-situ upgrading of oil shales, 2014. https://oaktrust.library.tamu.edu/handle/1969.1/153864 (accessed January 1, 2023).

(15) Song, X.; Zhang, C.; Shi, Y.; Li, G. Production performance of oil shale in-situ conversion with multilateral wells. *Energy* **2019**, *189*, 116145.

(16) Sun, Y.; Liu, Z.; Li, Q.; Deng, S.; Guo, W. Controlling groundwater infiltration by gas flooding for oil shale in situ pyrolysis exploitation. *J. Pet. Sci. Eng.* **2019**, *179*, 444−454.

(17) Torrente, M. C.; Galan, M. A. Kinetics of the thermal decomposition of oil shale from Puertollano (Spain). *Fuel* **2001**, *80* (3), 327−334.

(18) Abu El-Rub, Z.; Kujawa, J.; Al-Gharabli, S. Pyrolysis kinetic parameters of Omari oil shale using thermogravimetric analysis. *Energies* **2020**, *13* (16), 4060.

(19) Thakur, D. S.; Nuttall, H. E. Kinetics of pyrolysis of Moroccan oil shale by thermogravimetry. *Ind. Eng. Chem. Res.* **1987**, *26* (7), 1351−1356.

(20) Tiwari, P. Oil shale pyrolysis: Benchscale experimental studies and modeling. Ph.D. Dissertation, Department of Chemical Engineering, University of Utah, 2012 .

(21) Braun, R. L.; Burnham, A. K. Pmod: a flexible model of oil and gas generation, cracking, and expulsion. *Org. Geochem.* **1992**, *19* (1−3), 161−172.

(22) Pei, S.; Wang, Y.; Zhang, L.; Huang, L.; Cui, G.; Zhang, P.; Ren, S. An innovative nitrogen injection assisted in-situ conversion process for oil shale recovery: Mechanism and reservoir simulation study. *J. Pet. Sci. Eng.* **2018**, *171*, 507−515.

(23) Maes, J.; Muggeridge, A. H.; Jackson, M. D.; Quintard, M.; Lapene, A. Modelling in-situ upgrading of heavy oil using operator splitting method. *Comput. Geosci.* **2016**, *20*, 581−594.

(24) Reid, R. C.; Prausnitz, J. M.; Poling, B. E. *The properties of gases and liquids.* McGraw-Hill, 1987.

(25) Zeng, X.; Yao, C.; Zhao, X.; He, H. Thermal conductivity of N-pentadecane (C15H32). *Int. J. Thermophys.* **2019**, *40* (8), 72.

(26) (a) Selley, R. C., *Elements of petroleum geology.* Academic Press, San Diego. 1998. (b) Tiab, D.; Donaldson, E. C., Eds. *Petrophysics: Theory and practice of measuring reservoir rock and fluid transport properties.* Gulf Professional Publishing, 2014.

(27) Dullien, F. A. L. *Porous media: Fluid transport and pore structure.* Academic Press, 2nd ed. 1992.

(28) Ghasemi, M.; Astutik, W.; Alavian, S. A.; Whitson, C. H.; Sigalas, L.; Olsen, D.; Suicmez, V. S. Determining diffusion coefficients for carbon dioxide injection in oil-saturated chalk by use of a constant-volume-diffusion method. *SPE J.* **2017**, *22* (02), 505−520.

(29) Jia, B.; Tsau, J.-S.; Barati, R. A review of the current progress of CO_2 injection EOR and carbon storage in shale oil reservoirs. *Fuel* **2019**, *236*, 404−427.

(30) Li, Z.; Dong, M. Experimental study of carbon dioxide diffusion in oil-saturated porous media under reservoir conditions. *Ind. Eng. Chem. Res.* **2009**, *48* (20), 9307−9317.

(31) Bauman, J. H.; Deo, M. Simulation of a conceptualized combined pyrolysis, in situ combustion, and CO_2 storage strategy for fuel production from Green River oil shale. *Energy Fuels* **2012**, *26* (3), 1731−1739.

(32) CMG STARS User Guide. Thermal & Advanced Processes Simulator **2019**.